Gas Sensors

DOI: 10.1002/ange.200903926

Synthesis of Tin Dioxide Octahedral Nanoparticles with Exposed High-Energy {221} Facets and Enhanced Gas-Sensing Properties**

Xiguang Han, Mingshang Jin, Shuifen Xie, Qin Kuang, Zhiyuan Jiang, Yaqi Jiang, Zhaoxiong Xie,* and Lansun Zheng*

Tin dioxide (SnO_2), an n-type semiconductor with a wide band gap of 3.6 eV, has been widely used in photocatalytic degradation of organic dyes,[1] photovoltaic devices,[2] rechargeable lithium batteries,[3] and so on. In particular, remarkable receptivity to variations in gaseous environments and excellent chemical stability have made SnO_2 the best-known gas-sensing material.[4–9] Over the past decades, considerable efforts have been made to improve the sensitivity and selectivity of SnO_2-based solid-state gas sensors through modifying the sensing material itself and the fabrication technique, such as doping of catalytic metal particles,[4] hybridization of different sensing materials,[5,6] and optimization of working temperature.[7] In principle, gas sensing by metal-oxide semiconductors like SnO_2 is based on the oxidation–reduction reaction of the detected gases occurring on the semiconductor surface, which leads to an abrupt change in conductance of the sensor. For this reason, the gas-sensing ability of metal oxide semiconductors is in theory very sensitive to the crystal faces of the sensing materials.[10] From the viewpoint of chemical activity, metal-oxide nanocrystals with particular exposed crystal planes, such as high-index facets, may be good sensing materials, because high-index facets having high densities of atom steps, ledges, kinks, and dangling bonds usually exhibit much higher chemical activity.[11–13] However, such a strategy to improve sensitivity and selectivity of sensors has not attracted much attention up to now, possibly due to the difficulty of synthesizing metal-oxide nanocrystals with specific exposed crystal planes.

Herein we report a simple method for the preparation of octahedron-shaped SnO_2 with exposed high-index {221} facets by exploiting the coordinative-adsorption effect of HCl and poly(vinyl pyrrolidone), PVP, in solution. The {221} facets of SnO_2 have a higher relative surface energy (2.28 $J m^{-2}$) than common low-index facets such as {110} (1.401 $J m^{-2}$), {101} (1.554 $J m^{-2}$), and {100} (1.648 $J m^{-2}$).[14] As we expected, the as-prepared SnO_2 octahedra exhibit far better gas-sensing performance over ethanol than those mainly having exposed {110} facets.

Usually, a crystal prefers to expose crystal planes with low surface energy during growth. For example, both natural and synthetic forms of SnO_2 crystals are usually enclosed by {110}, {101}, or {100} facets with low surface energy.[10b] In recent years, special attention has been paid to developing methods to acquire nanocrystals with exposed high-energy surfaces, which usually show good chemical performance, for example, high catalytic activity.[11,15–19] Recently, Lu et al.[18] and we[19] prepared TiO_2 nanostructures with a large percentage of high-energy (001) facets, by taking advantage of the selective adsorption of fluoride ions. These results inspired us to synthesize other metal-oxide nanoparticles with high-energy crystal facets with the assistance of halide ions and other inorganic species.

The octahedral SnO_2 particles with high-index {221} facets were obtained through a hydrothermal route at 200 °C for 12 h, whereby $SnCl_4 \cdot 5H_2O$ was gradually hydrolyzed to form SnO_2 in an appropriate acidic environment adjusted with HCl in the presence of PVP. Figure 1a shows a typical powder X-ray diffraction (XRD) pattern of the as-prepared product, which can be indexed to the rutile phase of bulk SnO_2 with cell constants of $a = 4.738$ and $c = 3.187$ Å (JCPDS No. 41-1445). Scanning electron microscopy (SEM) showed that the product consists of high-purity particles with smooth surfaces (Figure 1b). These particles are of well-defined octahedral shape with an edge-to-edge width W of about 200 nm, and an apex-to-apex length L around 300 nm (see the inset of Figure 1b).

More-detailed structural information on the octahedral SnO_2 particles was provided by transmission electron micro-

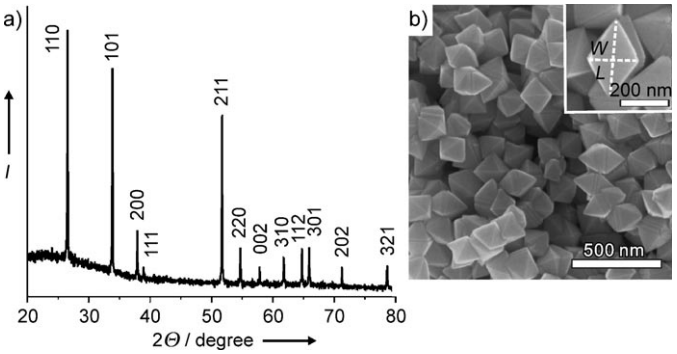

Figure 1. a) XRD pattern of the SnO_2 octahedra, b) typical SEM image of the SnO_2 octahedra.

[*] X. G. Han, M. S. Jin, S. F. Xie, Dr. Q. Kuang, Dr. Z. Y. Jiang, Y. Q. Jiang, Prof. Z. X. Xie, Prof. L. S. Zheng
State Key Laboratory for Physical Chemistry of Solid Surfaces
Department of Chemistry
College of Chemistry and Chemical Engineering, Xiamen University
Xiamen, 361005 (China)
Fax: (+86) 592-218-3047
E-mail: qkuang@xmu.edu.cn
zxxie@xmu.edu.cn

[**] This work was supported by the National Natural Science Foundation of China (Grant Nos. 20725310, 20721001, 20673085, and 20801045) and the National Basic Research Program of China (Grant Nos. 2007CB15303, 2009CB939804).

Supporting information for this article is available on the WWW under http://dx.doi.org/10.1002/anie.200903926.

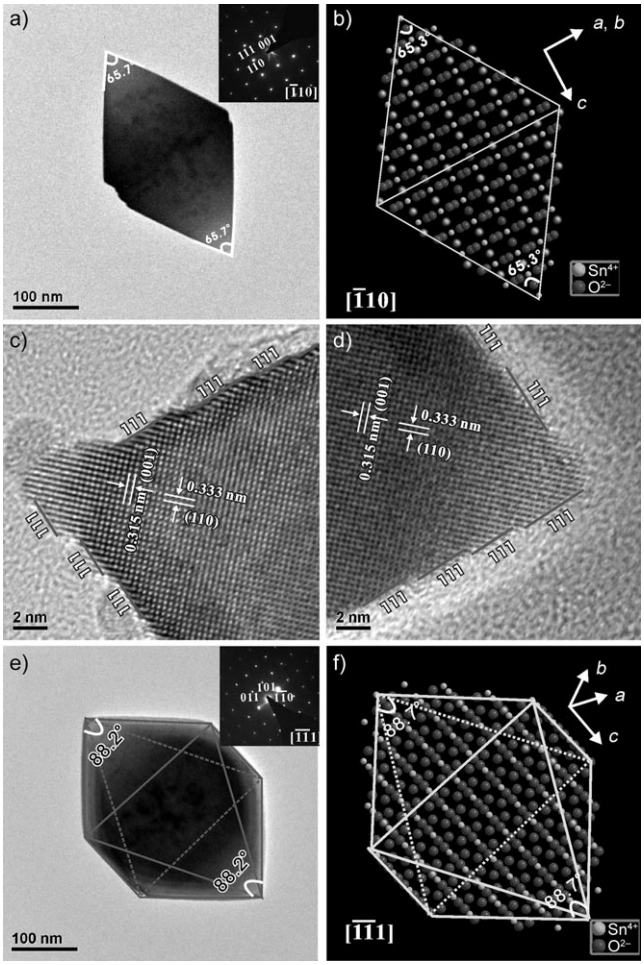

Figure 2. a) Typical low-magnification TEM image of an octahedral SnO_2 particle viewed along the [$\bar{1}$10] direction; inset: the corresponding SEAD pattern. b) Schematic model of an ideal SnO_2 octahedron enclosed within {221} facets, projected along the [$\bar{1}$10] direction. c) HRTEM image taken from the top apex of the octahedron. d) HRTEM image taken from the bottom apex of the octahedron. e) Low-magnification TEM image of the same SnO_2 octahedral particle viewed along the [$\bar{1}\bar{1}$1] direction; inset: the corresponding SAED pattern. f) Schematic model of an ideal SnO_2 octahedron enclosed within {221} facets, projected in the [$\bar{1}\bar{1}$1] direction.

scopy (TEM). Figure 2a shows a low-magnification TEM image of an individual octahedral particle, and the inset the corresponding selected-area electron diffraction (SAED) pattern. The SAED pattern can be indexed to the [$\bar{1}$10] zone axis of single-crystal tetragonal SnO_2, and this implies that the as-prepared octahedral SnO_2 particles are single-crystalline. Under electron-beam irradiation, the particle presents a diamond-like outline with an L/W ratio of about 1.5, and an apex angle between two side surfaces of about 65.7°. These structural features agree well with the model of octahedral SnO_2 enclosed by {221} facets projected along the [$\bar{1}$10] direction (Figure 2b). Structurally, a (221) surface can be described as combination of (111) terraces and (110) steps (see Figure S1, Supporting Information).[17a] In fact, such a stepped surface composed of (111) terraces and (110) steps was directly captured in high-resolution TEM (HRTEM) images recorded from the top and bottom apexes of the octahedron (Figure 2c and d).

To further confirm the identity of the exposed surfaces of the octahedral SnO_2, the same particle was rotated to the [$\bar{1}\bar{1}$1] zone axis from the [$\bar{1}$10] zone axis. As shown in Figure 2e and f, both the outline and the apex angle of the particle still correspond well with the octahedral SnO_2 model enclosed by {221} facets, projected along the same direction (Figure 2f). On the basis of the above TEM observations and structural analysis, we conclude that the exposed surfaces of the as-prepared octahedral SnO_2 particles are the {221} facets. There are obvious morphological differences between the SnO_2 octahedra with exposed {221} facets and octahedra bound by {111} facets. The latter have a larger apex angle and smaller L/W ratio when projected along the same direction (see Figure S2 of the Supporting Information for the structural model of an octahedron bound by {111} facets).

In the synthetic method, adding an appropriate amount of hydrochloric acid is crucial for the formation of octahedral SnO_2 particles enclosed by {221} facets. In fact, perfect octahedral SnO_2 particles can only be obtained within a narrow window of acidity (adding 0.60 mL of HCl to the solution (6 mL), pH 0.4). When the amount of HCl added is increased to 0.8 mL, hydrolysis of Sn^{4+} is completely inhibited and thus no product can be obtained. When the amount of HCl added is decreased from 0.60 to 0.40 mL, the formed SnO_2 particles evolve into elongated octahedra (Figure 3a). The HRTEM and SEAD characterization (Figure S3, Supporting Information) demonstrates that the middle parts of these elongated octahedra are bound by low-energy {110} facets, and the pyramidal tips by stepped high-energy {221} facets. According to the geometry of the elongated octahedral SnO_2 particles, the percentage of exposed {221} facets is estimated as about 56%. When the amount of HCl added is further decreased to 0.2 mL, tetragonal SnO_2 nanorods with two pyramidal tips are mainly formed (Figure 3b). For such lancelike SnO_2 nanorods, the low-energy {110} facets are dominant, and the high-energy {221} facets only account for 13% of the total exposed surface (see Figure S4 in the Supporting Information for a more detailed HRTEM characterization).

These preliminary results indicate that the octahedral SnO_2 particles enclosed within {221} surfaces result from the coordinative effect of H^+ and Cl^-. Tin(IV) ions are easily hydrolyzed in aqueous solution to produce extremely small SnO_2 particles (see Figure S5, Supporting Information).

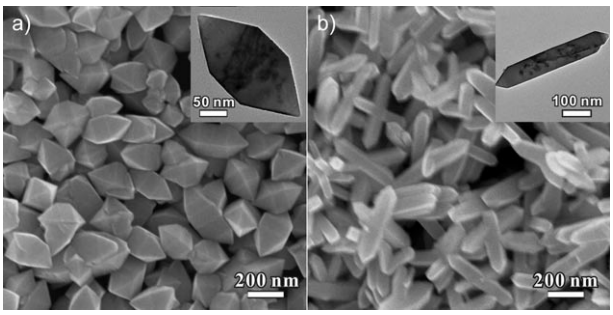

Figure 3. SEM images of SnO_2 particles synthesized by hydrolysis of $SnCl_4{\cdot}5H_2O$ (0.350 g, 1 mmol) by adding a) HCl (0.40 mL, 37.5%) and PVP (0.315 g, 0.006 mmol), b) HCl (0.20 mL, 37.5%) and PVP (0.315 g, 0.006 mmol).

Addition of HCl solution can inhibit hydrolysis of Sn^{4+} ions to a certain extent and slow down the growth of SnO_2 nanocrystals, and this provides an opportunity to kinetically control the shape of the SnO_2 nanocrystals by specific adsorption of Cl^- ions. The PVP surfactant plays a key role in dispersing the SnO_2 particles, rather than in morphology control. The SnO_2 particles obtained without PVP are still octahedra, but they aggregate with each other (Figure S6, Supporting Information).

Since the {221} facets have high-density atom steps, ledges, and dangling bonds, the as-synthesized octahedral SnO_2 particles are anticipated to show good performance in gas sensing. In our experiments, ethanol was used as probe molecule to investigate gas-sensing properties of the materials, and the lance-shaped and elongated-octahedral SnO_2 particles were used as references for comparison. Figure 4a shows sensing sensitivity curves of the three kinds of SnO_2 particles as a function of ethanol concentration. In the gas-sensing tests, all SnO_2 samples had the same weight for convenience of comparison. The sensitivity of the octahedral SnO_2 particles is much higher than those of the other two SnO_2 samples. With regard to the shapes of these samples (Figure 4b–d), the sensing activity is proportional to the percentage of {221} facets among the exposed surfaces. For example, at an ethanol concentration of 200 ppm, the octahedral SnO_2 particles have a sensitivity of up to 150, while the sensitivity is about 50 for the elongated-octahedral SnO_2 particles, and only 20 for the lance-shaped SnO_2 particles.

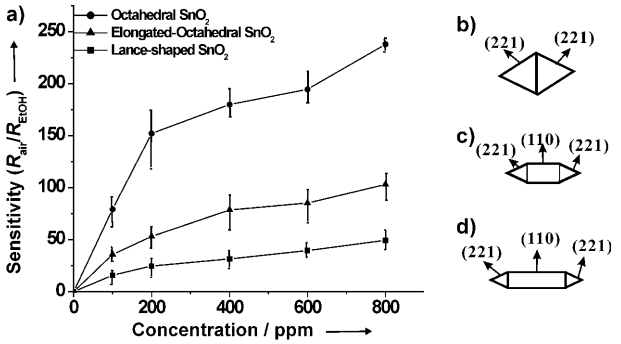

Figure 4. a) Sensitivity curves of SnO_2 particles of different shapes as a function of ethanol concentration. R = resistance. b)–d) Morphological models for the octahedral, elongated-octahedral, and lance-shaped SnO_2 particles.

Gas-sensing performance is also affected by the surface area, and a larger surface area usually leads to better sensing properties. However, in the present case, the octahedral particles are clearly larger than the elongated-octahedral and lance-shaped particles, that is, the octahedral particles have the smallest surface area. Brunauer–Emmett–Teller (BET) measurements further confirmed that the octahedral particles have the lowest surface area among the three SnO_2 shapes. The specific surface areas were measured to be 11.02 m^2g^{-1} for the octahedral particles, 18.70 m^2g^{-1} for the elongated-octahedral particles, and 41.49 m^2g^{-1} for the lance-shaped particles. After normalization with their BET surface areas, the order of gas-sensing performance of the three kinds of SnO_2 particles does not change (Figure S7, Supporting Information). A similar phenomenon was found for the detection of other alcohols, such as methanol (Figure S8, Supporting Information) and 2-propanol (Figure S9, Supporting Information), where the octahedral particles also showed the best sensing properties. The results indicate that the superior gas-sensing performance of the octahedral particles is not due to the surface area, but to the nature of the material, which is correlated with the surface structure. In other words, the {221} facets of SnO_2 have better gas-sensing properties than the {110} facets.

It is well accepted that the sensing mechanism of metal-oxide semiconductors like SnO_2 involves an adsorption–oxidation–desorption process in which chemisorbed oxygen plays a crucial role. Since electrons are transferred from the crystal bulk to chemisorbed oxygen, an electron-depletion layer is formed on the surface of the sensing material and leads to high resistance of the sensor. When the sensor is exposed to an analyte gas (here ethanol), ethanol molecules are oxidized by surface-adsorbed ionized oxygen species (e.g., O_2^-, O^{2-}, O^-) to aldehyde through catalytic interaction with the SnO_2 surface.[20,21] The oxidation reactions produce more electrons and thus increase the conductivity of the sensor. The adsorption of oxygen species is closely related to structural defects on the surface, especially oxygen vacancies. For SnO_2 particles with the same surface area, therefore, the sensitivity of the sensing material depends on the surface defects of the different crystal planes.

Figure 5 shows schematic models of SnO_2 (110) and (221) surfaces that contain several atom steps. For rutile SnO_2, Sn atoms in the bulk are sixfold-coordinated by O atoms. At the surface, tin atoms are usually coordinatively unsaturated. As shown in Figure 5a, the rutile (110) surface contains rows of sixfold-coordinated Sn atoms (blue) and fivefold-coordinated Sn atoms (yellow) with one dangling bond perpendicular to the surface.[14] On the (221) surface, however, all Sn atoms are coordinatively unsaturated, located in fivefold-coordinated sites (yellow) with one dangling bond and fourfold-coordinated sites (green) with two dangling bonds (Figure 5b). Thus, there are more dangling bonds on the (221) surface than on the (110) surface. This suggests that the (221) facet of SnO_2 is highly active for adsorption of ionized oxygen species, which will greatly improve the response of SnO_2 to the detected gas. The discussion above accounts for the high performance of the as-prepared octahedral SnO_2 particles enclosed within {221} facets in comparison with SnO_2 particles with exposed stable {110} facets.

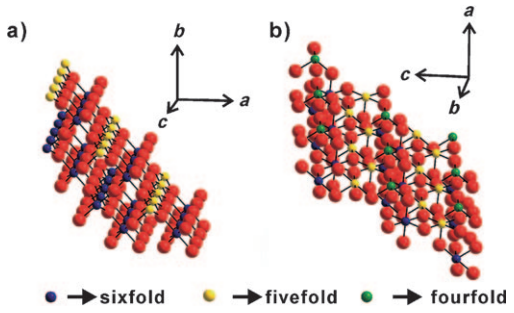

Figure 5. Schematic models of a) the (110) surface and b) the (221) surface.

In summary, octahedral SnO_2 particles with exposed high-energy {221} facets were synthesized by a simple hydrothermal route with the assistance of HCl and PVP. The morphologies (lance-shaped, elongated-octahedral, octahedral) of the SnO_2 particles can be controlled by changing the amount of HCl. The octahedral SnO_2 particles show excellent gas-sensing performance due to the high chemical activity of the exposed {221} facets. Our results demonstrate that it is feasible to improve gas-sensing properties of SnO_2-based sensors by the surface-engineering strategy, that is, selectively exposing high-energy facets at the surface of sensing materials. In addition, the present study motivates us to further explore new synthetic methods for the preparation of other metal oxides with a high percentage of reactive facets, which have promising applications as gas sensors, photocatalysts, solar cells, and optoelectronic devices.

Experimental Section

Reagents: $SnCl_4{\cdot}5H_2O$, hydrochloric acid (37.5%), and PVP (K-30) were purchased from Sinopharm Chemical Reagent (Shanghai, China). All reagents were used as received.

Synthesis and characterization of SnO_2 octahedra: In a typical synthesis, $SnCl_4{\cdot}5H_2O$ (0.350 g, 1 mmol), HCl (0.60 mL), and PVP (0.315 g, 0.006 mmol) were added in order to ethanol/distilled water (6.00 mL, 1/1 v/v) under intense ultrasonic treatment. The resulting solution was transferred to a Teflon-lined stainless steel autoclave and kept at 200 °C for 12 h. The products were collected by centrifugation at 4000 rpm, and washed several times with deionized water and ethanol. The lance-shaped and elongated-octahedral SnO_2 were synthesized in a similar way except that 0.20 and 0.40 mL of HCl were used instead of 0.60 mL HCl, respectively.

The composition and phase of the as-prepared products were determined by means of the powder XRD pattern, recorded on a Panalytical X-pert diffractometer with $Cu_{K\alpha}$ radiation. The morphology and crystal structure of the as-prepared products were observed by SEM (S4800) and HRTEM (FEI Tecnai-F30) with an acceleration voltage of 300 kV. All TEM samples were prepared by depositing a drop of diluted suspension in ethanol on a copper grid coated with carbon film. The surface areas of the three types of SnO_2 particles with different shapes were measured by the BET method by measuring nitrogen-adsorption and -desorption isotherms on a Micrometrics ASAP 2020 system.

Gas-sensing test on the SnO_2 octahedra: The gas-sensing tests were performed in a WS-30A measuring system (Zhengzhou Winsen Electronics Technology, China).[13] In a typical test, a gas sensor was fabricated by coating a certain amount of SnO_2 paste (consisting of SnO_2 particles and the ethanol solvent) onto a ceramic tube that was previously mounted with gold electrodes and platinum conducting wires. A resistor wire coil was inserted in the tube as a heater to provide working temperatures from 200 to 500 °C by varying the heating current. The analytes were injected either directly into the chamber or, in the case of liquids like ethanol, onto a metal-plate heater in the test chamber and evaporated completely by heating. The gas-sensing capability of the sensor was defined as the ratio R_{gas}/R_{air}, where R_{gas} and R_{air} are the electrical resistance of the sensor in test gas and in air at the working temperature of about 350 °C, respectively.

Received: July 17, 2009
Revised: September 21, 2009
Published online: October 23, 2009

Keywords: hydrothermal synthesis · nanoparticles · sensors · surface engineering · tin dioxide

[1] a) J. P. Wilcoxon, *J. Phys. Chem. B* **2000**, *104*, 7334; b) G. Wang, W. Lu, J. H. Li, J. Choi, Y. Jeong, S. Y. Choi, J. B. Park, M. K. Ryu, K. Lee, *Small* **2006**, *2*, 1436.
[2] a) J. Y. Kim, I. J. Chung, J. K. Kim, J. W. Yu, *Curr. Appl. Phys.* **2006**, *6*, 969; b) S. Gubbala, V. Chakrapani, V. Kumar, M. K. Sunkara, *Adv. Funct. Mater.* **2008**, *18*, 2411.
[3] a) M. S. Park, G. X. Wang, Y. M. Kang, D. Wexler, S. X. Dou, H. K. Liu, *Angew. Chem.* **2007**, *119*, 764; *Angew. Chem. Int. Ed.* **2007**, *46*, 750; b) H. Kim, J. Cho, *J. Mater. Chem.* **2008**, *18*, 771.
[4] a) P. Manjula, L. Satyanarayana, Y. Swarnalatha, S. V. Manorama, *Sens. Actuators B* **2009**, *138*, 28; b) G. Korotcenkov, B. K. Cho, L. Gulina, V. Tolstoy, *Sens. Actuators B* **2009**, *138*, 512; c) V. Kumar, S. Sen, K. P. Muthe, N. K. Gaur, S. K. Gupta, J. V. Yakhmi, *Sens. Actuators B* **2009**, *138*, 587.
[5] a) A. F. Chen, S. L. Bai, B. J. Shi, Z. Y. Liu, D. Q. Li, C. L. Chung, *Sens. Actuators B* **2008**, *135*, 7; b) Y. J. Chen, C. L. Zhu, L. J. Wang, P. Cao, M. S. Cao, X. L. Shi, *Nanotechnology* **2009**, *20*, 045502.
[6] a) Q. Kuang, C. S. Lao, Z. Li, Y. Z. Liu, Z. X. Xie, L. S. Zheng, Z. L. Wang, *J. Phys. Chem. C* **2008**, *112*, 11539; b) X. F. Song, Z. J. Wang, Y. B. Liu, C. Wang, L. J. Li, *Nanotechnology* **2009**, *20*, 075501.
[7] a) J. R. Huang, G. Y. Li, Z. Y. Huang, X. J. Huang, J. H. Liu, *Sens. Actuators B* **2006**, *114*, 1059; b) V. V. Malyshev, A. V. Pislyakov, *J. Anal. Chem.* **2009**, *64*, 90.
[8] A. Köck, A. Tischner, T. Maier, M. Kast, C. Edtmaier, C. Gspan, G. Kothleitner, *Sens. Actuators B* **2009**, *138*, 160.
[9] J. Q. Xu, D. Wang, L. P. Qin, W. J. Yu, Q. Y. Pan, *Sens. Actuators B* **2009**, *137*, 490.
[10] a) M. Batzill, *Sensors* **2006**, *6*, 1345; b) M. Batzill, K. Katsiev, J. M. Burst, U. Diebold, A. M. Chaka, B. Delley, *Phys. Rev. B* **2005**, *72*, 165414; c) J. D. Prades, A. Cirera A. J. R. Morante, *J. Electrochem. Soc.* **2007**, *154*, H675.
[11] a) N. Tian, Z. Y. Zhou, S. G. Sun, Y. Ding, Z. L. Wang, *Science* **2007**, *316*, 732; b) N. Tian, Z. Y. Zhou, S. G. Sun, *J. Phys. Chem. C* **2008**, *112*, 19801; c) N. Tian, Z. Y. Zhou, S. G. Sun, *Chem. Commun.* **2009**, 1502.
[12] a) X. W. Xie, Y. Li, Z. Q. Liu, M. Haruta, W. J. Shen, *Nature* **2009**, *458*, 746; b) L. H. Hu, Q. Peng, Y. D. Li, *J. Am. Chem. Soc.* **2008**, *130*, 16136.
[13] X. G. Han, H. Z. He, Q. Kuang, X. Zhou, X. H. Zhang, T. Xu, Z. X. Xie, L. S. Zheng, *J. Phys. Chem. C* **2009**, *113*, 584.
[14] B. Slater, C. R. A. Catlow, D. H. Gay, D. E. Williams, V. Dusastre, *J. Phys. Chem. B* **1999**, *103*, 10644.
[15] a) Z. Y. Jiang, T. Xu, Z. X. Xie, Z. W. Lin, X. Xu, R. B. Huang, L. S. Zheng, *J. Phys. Chem. B* **2005**, *109*, 23269; b) T. Xu, X. Zhou, Z. Y. Jiang, Q. Kuang, Z. X. Xie, L. S. Zheng, *Cryst. Growth Des.* **2009**, *9*, 192.
[16] D. B. Fan, P. J. Thomas, P. O'Brien, *J. Am. Chem. Soc.* **2008**, *130*, 10892.
[17] a) Y. Y. Ma, Q. Kuang, Z. Y. Jiang, Z. X. Xie, R. B. Huang, L. S. Zheng, *Angew. Chem.* **2008**, *120*, 9033; *Angew. Chem. Int. Ed.* **2008**, *47*, 8901; b) H. G. Liao, Y. X. Jiang, Z. Y. Zhou, S. P. Chen, S. G. Sun, *Angew. Chem.* **2008**, *120*, 9240; *Angew. Chem. Int. Ed.* **2008**, *47*, 9100.
[18] a) H. G. Yang, C. H. Sun, S. Z. Qiao, J. Zou, G. Liu, S. C. Smith, H. M. Cheng, G. Q. Lu, *Nature* **2008**, *453*, 638; b) H. G. Yang, G. Liu, S. Z. Qiao, C. H. Sun, Y. G. Jin, S. C. Smith, J. Zou, H. M. Cheng, G. Q. Lu, *J. Am. Chem. Soc.* **2009**, *131*, 4078.
[19] X. G. Han, Q. Kuang, M. S. Jin, Z. X. Xie, L. S. Zheng, *J. Am. Chem. Soc.* **2009**, *131*, 3152.
[20] D. Kohl, *Sens. Actuators* **1989**, *18*, 71.
[21] T. Kinkawa, G. Sakai, J. Tamaki, N. Miura, N. Yamazoe, *J. Mol. Catal. A* **2000**, *155*, 193.

